

COMPREHENSIVE INVESTIGATION MODELING FOR SEMICONDUCTOR OPTICAL AMPLIFIER (SOA)

Esra A. Alquda¹ and Aser M. Matarneh²

Department of Electrical Engineering, Mutah University, Jordan.
aser_m2002@yahoo.com¹, aser.matarneh@mutah.edu.jo²

(Received: 03-Oct.-2015, Revised: 22-Dec.-2015, Accepted: 28-Dec.-2015)

ABSTRACT

This paper presents the effects of the input signal on the gain and carrier density response of a semiconductor optical amplifier (SOA). The SOA is modeled using a segmentation method. The input bias current input power, wavelength and the length of SOA required for amplification and switching functions are investigated. Moreover, the effect of temperature on SOA operation is investigated, as well as the thermo-optical effect. The operation principle is simulated, and the results show the input boundary conditions and requirements in which the SOA can be used as an amplifier and as a switch.

KEYWORDS

Semiconductor optical amplifier (SOA), Carrier density, Stimulated emission, Gain response, Thermo-optical effect, Dynamic range, Phase shift, Linear region.

1. INTRODUCTION

As the demand for network capacity is rising due to the rapid increase in the Internet traffic volume, there is a growing need for all-optical based systems. The all-optical based system should offer much greater bandwidth and higher reliability than the traditional copper cables and the optoelectronic based communication technologies.

In the beginning, optical fiber network started as a simple connection with no routing capability. The use of wavelength division multiplexing (WDM) and optical time division multiplexing (OTDM) increased the overall capacity of the point-to-point optical fiber transmission systems.

The development of second-generation high speed systems, such as the synchronous optical network and the synchronous digital hierarchy, offered supplementary switching and routing capabilities to the network [1]-[2]. Optical add/drop multiplexers and optical cross connectors were further introduced to the network in order to offer wavelength routing capabilities [3]-[4]. However, in such systems, the switching process is still performed in the electrical domain requiring optical-electrical-optical (O-E-O) conversion modules [5]-[6]. To meet the network speed and capacity demands and to overcome the bottlenecks of O-E-O conversion, ultra-fast photonic networks that rely on photonic signal processing are required. The next generation optical network is aimed to carry out all the processing in the optical domain, operating at speeds (hundreds of gigabits per second) well beyond the existing electronic devices [7]-[12]. It is important to note that an all-optical processing technology is not a replacement, but is a complementary alternative, to electrical processing, particularly at the backbone optical layer. Both circuit and packet switching could be adopted in all- optical networks.

However, packet switching is more flexible than circuit switching in throughput and switching speed [13]. An all-optical network offers transparency, implying that data can be carried at a range of bit rates and protocols and can also support different higher layers.

The development of high capacity optical networks increased the demand for new optical devices that are able to perform in almost all-optical functions. The key processes in all-optical switching are regeneration and wavelength conversion, where SOA is the key building block. Among all-optical switches [14], ultra-fast all-optical switches based on the SOA, such as Mach-Zehnder interferometers (MZI) [15]-[21] are the most promising candidates for the realization of all-optical switching and processing applications compared to other switches, such as ultra-fast non-linear interferometers (UNIs) [22]-[23] and terahertz optical asymmetric demultiplexers (TOADs) [24]-[26].

The use of SOA-based Mach-Zehnder interferometer (SOA-MZI) schemes will allow the processing of packets 'on-the-fly' in future photonic routers. The SOA-MZI is used in almost all functions inside a photonic router, such as clock extraction circuits, header/payload separation, optical flip-flops, wavelength converters, all-optical gates and switching [27]-[34]. The performance of SOA, in terms of the gain temporal behavior, the carrier density and stimulation emission, is affected by several factors, including the dimensions of the waveguide and input parameters, such as the external bias current and the power and wavelength of the propagating input signal. Controlling these factors will lead to improving and optimizing the SOA amplification and/or switching characteristics, as well as the uniformity of the generated output signal that is necessary to reduce the system power penalty.

This paper proposes a segmentation model of the SOA based on numerical and mathematical equations. The model is used to analyze the impact of the input parameters and propagating signals on the SOA carrier density and its gain response to further understand the SOA operation. The segmentation model has been introduced in modeling the semiconductor devices [35]. However, the segmentation model used in this paper takes into account the differential gain effect and the temperature effect of the semiconductor optical amplifier. It also investigates switching operation in more details. Moreover, the dynamic behavior of SOA, including optical-thermo-effect and dynamic range will be thoroughly investigated.

Next stage will be dealing with optimization of SOA parameters to maximize the output gain for amplification and optimization of SOA non-linear characteristics when used in optical switching. The boundaries and conditions necessary for the input parameters to achieve the 180° induced phase shift are managed for switching function in SOA-based optical switches.

The paper is organized as follows; in the next section, the principle of SOA is presented. Section three introduces the mathematical model used, including segmentation model and rate equations of SOA with phase shift equations. Section four presents the results and discussion. The conclusion is then drawn.

2. PRINCIPLE OF SOA

SOAs amplify incident light through stimulated emission. An electrical pump current is used to excite the electrons in the active region of the SOA. When the optical signal travels through the active region, it causes these electrons to lose energy in the form of photons and get back to the ground state. The stimulated photons have the same wavelength as the optical signal, thus amplifying the optical signal as shown in Figure 1. The basic working principle of a SOA is the same as a semiconductor laser, but without feedback.

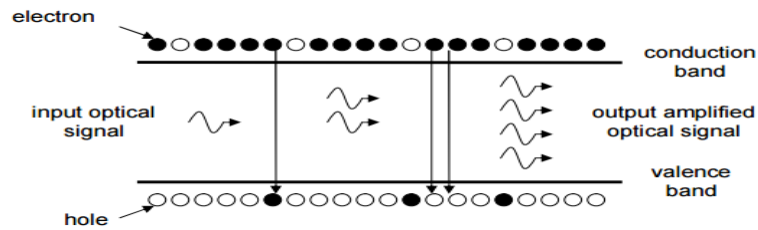


Figure 1. SOA amplifications due to stimulation emission process [36].

3. METHOD

3.1 Segmentation Model

In order to understand the factors affecting the SOA gain and the emerging output signals, a segmentation model of the SOA is introduced, where the SOA is divided into ten equal segments of length $l=L/10$ each. The model helps in identifying the small changes that occur within the short length of each segment. Ten segments were chosen for a sufficient accurate investigation on the change in the carrier density and the signal gain along the SOA.

3.2 Mathematical Model

The rate equations in small segments in an SOA are iteratively calculated while taking the carrier density change and the SOA length into account [37].

3.2.1 Rate Equations

When light is injected into the SOA, changes occur in the carrier and photon densities within the active region of the SOA. These changes can be described using the rate equations. The gain medium of the amplifier is described by the material gain coefficient, g (per unit length) which is dependent on the carrier density N and is given by [38]:

$$g = a_1 (N - N_0); \quad (1)$$

where N_0 is the carrier density at transparency point and a_1 is the differential gain parameter. The net gain coefficient g_t is defined by:

$$g_t = \Gamma \cdot g - a_s \quad (2)$$

where a_s is the internal waveguide scattering loss and Γ is the confinement factor, which is the ratio of the light intensity within the active region to the sum of light intensity [39]. The total gain G of an optical wave experienced at the location z of an SOA can be calculated according to:

$$G = e^{g_t \cdot z} \quad (3)$$

assuming a constant carrier density at any given location z within the active region of the SOA. Therefore, the average output power P_{av} over the length of the SOA becomes:

$$P_{av} = P_{in} \frac{(e^{g_t \cdot L} - 1)}{g_t \cdot L} \quad (4)$$

where L is the length of the SOA and P_{in} is the input signal power. The carrier density rate equation expresses the conservation of carriers inside the active layer. It takes into account the current density and the net rate of carrier generation and recombination averaged over the active layer. The recombination rate consists of spontaneous and stimulated recombination. The spontaneous recombination rate includes the radiative and non-radiative components. The non-radiative recombination takes into account the Auger recombination, which is generally the

dominant non-radiative process in long wavelength lasers. The dynamic equation for the change in the carrier density within the active region of the device is given by:

$$\frac{dN}{dt} = \frac{I_{dc}}{q \cdot V} - R(N) - \frac{\Gamma \cdot g \cdot P_{av} \cdot L}{V \cdot h \cdot f} \quad (5)$$

where I_{dc} is the DC bias current injected to the SOA, q is the electron charge and V is the active volume of the SOA:

$$V = L \cdot H \cdot W \quad (6)$$

where W and H denote the width and the thickness of the active region, respectively. $R(N)$ is the recombination rate, h is the Planck constant and f is the light frequency. The definition for $R(N)$ used in this model is given by:

$$R(N) = A \cdot N + B \cdot N^2 + C \cdot N^3 \quad (7)$$

where A is the non-radiative coefficient recombination at defects and traps, B is the spontaneous radiative recombination coefficient and C is the Auger recombination coefficient. The cubic equation is the best to fit the real gain coefficient g . The material gain coefficient depends on both the carrier density N and the input signal wavelength λ and can be rewritten as [40]:

$$g = \frac{a_1(N - N_0) - a_2(\lambda - \lambda_N)^2 + a_3(\lambda - \lambda_N)^3}{1 + \epsilon \cdot P_{av}} \quad (8)$$

where a_2 and a_3 are empirically determined constants that are chosen to fit an experimentally measured SOA gain curve. λ_N is the peak gain wavelength and ϵ is the gain compression factor. The peak gain wavelength is given by:

$$\lambda_N = \lambda_0 - a_4(N - N_0) \quad (9)$$

where λ_0 is the peak gain wavelength at transparency and a_4 denotes the empirical constant that shows the shift of the gain peak.

3.2.2 Phase Shift Equations

Changes in the carrier density take place with the propagation of the input signal pulse through the SOA, hence affecting its propagation coefficient (via the non-linear refractive index variations in the SOA active region). Because of the finite carrier lifetime, the leading edge of the input pulse experiences a different phase shift relative to the lagging edge. This process is (SPM). Let Δn represent the effective refractive index variation within the active region [39]:

$$\Delta n = \Gamma \cdot \frac{dn}{dN} \cdot (N - N_{ss}) \quad (10)$$

where dn/dN is the refractive index shift coefficient and N_{ss} is the carrier density at steady state (i.e., with no input signal launched to the biased SOA). The total phase shift experienced by the propagating input signal is [40]:

$$\Delta \phi = \int_0^L \left(\frac{2\pi}{\lambda} \cdot \Delta n \right) \cdot dz \quad (11)$$

A thermo-optical effect is a change in the optical properties of a material in response to temperature. The thermo-optical effect may eventually lead to unstable operation of the SOA, since the effective refractive index changes as a function of temperature. A linear approximation for the effective refractive index as a function of temperature is given as shown below [41]:

$$n(T) = n_0 + \frac{\Delta n}{\Delta T} (T - T_0) \quad (12)$$

where n_0 is the refractive index at room temperature, T_0 . n_0 for silicon device is 3.48314 [42]. $\left(\frac{\Delta n}{\Delta T}\right)$ is the index variation with temperature (thermo-optical coefficient).

The total phase shift experienced by the propagating input signal is [40]:

$$\Delta \phi = \int_0^L \left(\frac{2\pi}{\lambda} \cdot n(T) \right) \cdot dz \quad (13)$$

4. RESULTS AND DISCUSSION

The rate equations shown in the previous section are derived via Matlab to investigate the gain response of the SOA model while employing the segmentation method. The standard SOA parameters used are given in Table 1. The segmentation method involves dividing the SOA into ten equal segments of length $l=L/10$ each. The carrier density is assumed to be constant within a segment. However, the carrier density changes from one segment to another depending on its input power and the carrier density of the previous segment using equation (5). In all of the equations, the segment length l will replace the SOA length L for segment total gain and carrier density calculations.

Figure 2 shows the dynamic range of a semiconductor optical amplifier (SOA); that is the input power range within which an SOA can be operated error free. It is among the most important parameters describing the usability range of an SOA in an access network. Figure 3 shows the normalized gain response of the SOA using the physical parameters in Table 1. As it can be seen, the gain of the SOA increases rapidly up to a steady state value, where it becomes almost constant. This increase is due to the injection of the bias current to the SOA, hence resulting in a large number of electrons to overcome the energy gap to reach the conduction band.

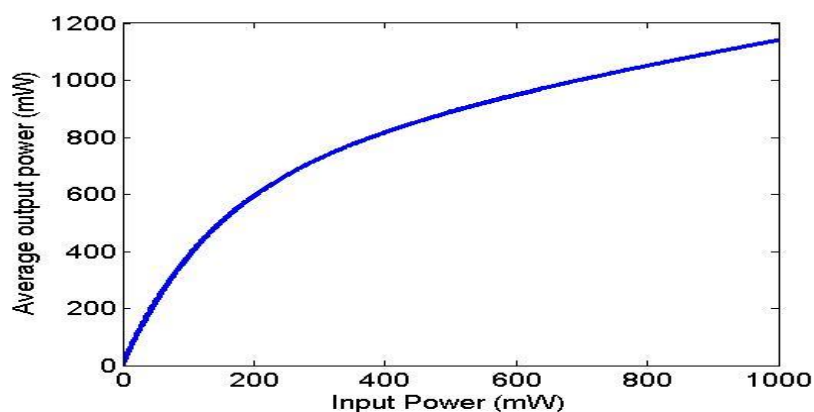


Figure 2. Dynamic range of SOA.

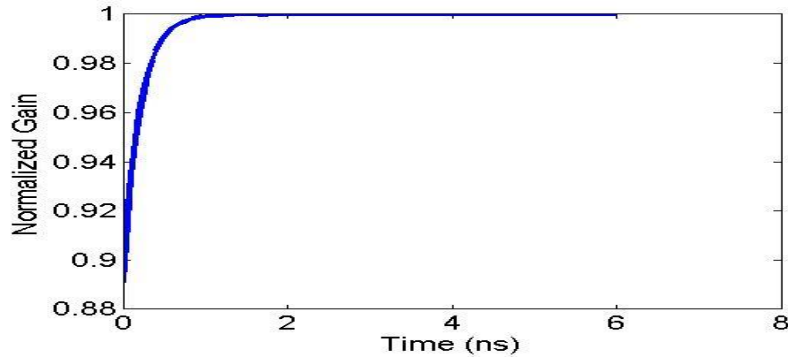


Figure 3. The Normalized gain response of the SOA with no input signal.

Table 1. Physical parameters of the SOA.

Parameter	Value
Carrier density at transparency (N_0)	$1.4 \times 10^{24}/m^3$
Initial carrier density (N_i)	$3 \times 10^{24}/m^3$
Wavelength at transparency (λ_0)	1605nm
Initial waveguide scattering loss (a_s)	$40 \times 10^2/m$
Differential gain (a_1)	$2.78 \times 10^{-20} m^2$
Gain constant (a_2)	$7.4 \times 10^{18}/m^3$
Gain constant (a_3)	$3.155 \times 10^{25}/m^4$
Gain peak shift coefficient (a_4)	$3 \times 10^{-32} m^4$
SOA length (L)	500 μm
SOA width (W)	3 μm
SOA height (H)	80 nm
Confinement factor (Γ)	0.3
Surface and defect recombination coefficient (A)	$3.6 \times 10^8/s$
Radiative recombination coefficient (B)	$5.6 \times 10^{-16} m^3/s$
Auger recombination coefficient (C)	$3 \times 10^{-41} m^6/s$
Gain compression factor (ϵ)	$0.2/W$
Equivalent refractive index (n_{eq})	3.5
Differential of equivalent refractive index with respect to carrier density (dn/dN)	$-1.2 \times 10^{-26}/m^3$
Index variation with temperature ($\frac{\Delta n}{\Delta T}$)	$10^{-4}/K$

4.1 Amplification

In order to use the SOA as an amplifier, it is necessary to ensure that the signal will not be affected by the SOA non-linear response that occurs when the SOA gain reaches its saturation value as shown in Figure 4, where the SOA decreases sharply to the saturation level. The reason for such response is that a depletion of the carrier density happens due to the continuous

stimulation emission process. A range of input pulse signals with optical power values from 1 mW to 10 mW were applied to the SOA, and the signal output gains are illustrated in Figure 5.

As it can be seen from Figure 5, the simulated result is in clear agreement with the measured result. As expected, the figure shows that, for both curves, at a fixed wavelength, the gain gradually decreases with increasing the input power level. This effect is because a signal with higher power will interact with a larger number of excited electrons in the conduction band, thus resulting in increased depletion in the carrier density and the SOA gain. This process is applied for 1550 nm wavelength. As it can be noted from 1 mW input power at measured and simulated curves, the gain values obtained are 100 and 98 respectively; where it should be noted that the small discrepancy between the measured and simulated curves is due to simulation accuracy.

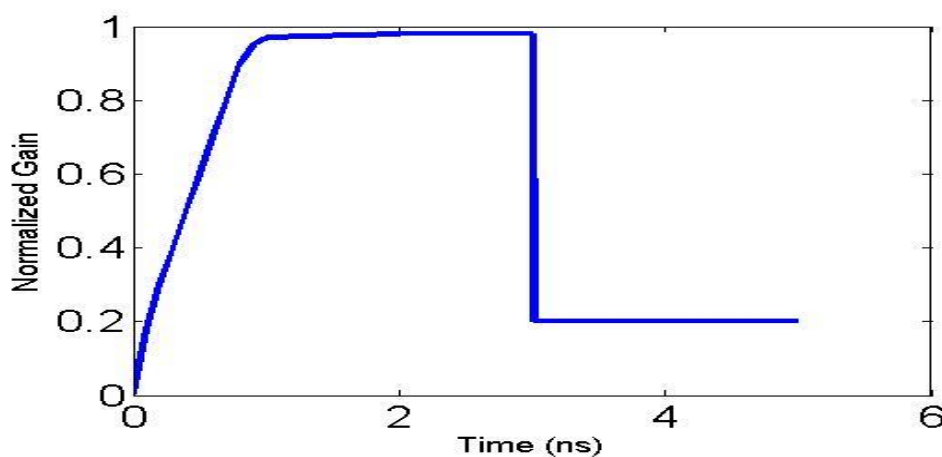


Figure 4. Normalized gain response of the SOA due to continuous wave (CW) probe.

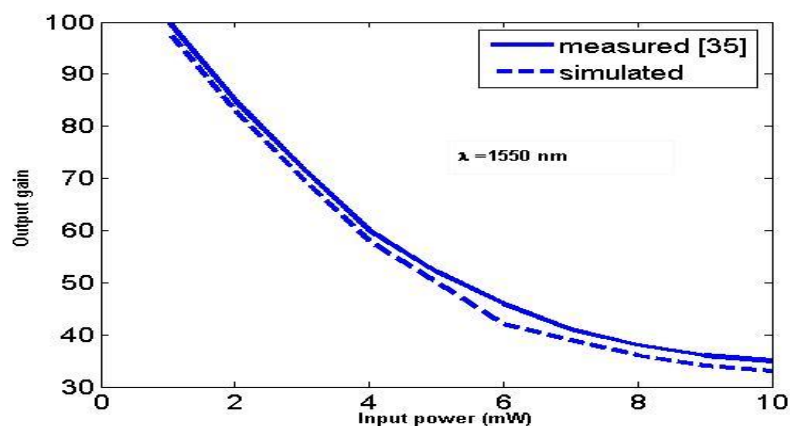


Figure 5. Signal output gain corresponding to the input power at a wavelength of 1550 nm.

4.2 Input Signal Wavelength Investigation

The wavelength of the input signal has a direct impact on the SOA gain as can be seen from the third order gain coefficient equation. The depletion of the SOA gain that occurs due to the injection of input signal is directly related to the input power. Therefore, in order to understand these effects, the SOA gain as a function of the input power, for a range of wavelengths in the C-band (1530 to 1565 nm), is illustrated in Figure 6. As expected, the SOA gain reduces with increasing the input signal power at all wavelengths. This gain reduction is because a signal

with higher power level will interact with a larger number of excited electrons in the conduction band, thus resulting in higher depletion of the carrier density and the SOA gain. From the figure, it is observed that at lower wavelengths, lower gains are achieved.

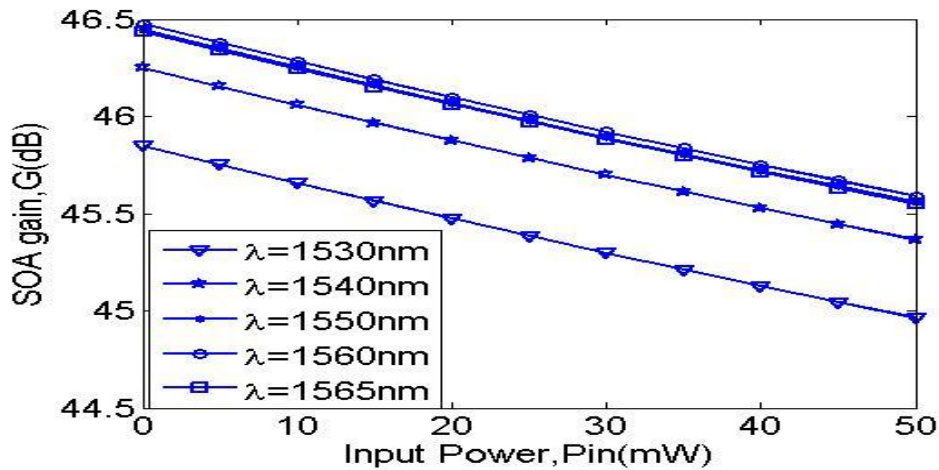


Figure 6. SOA gain as a function of input signal power when operated in the C- band.

4.3 Applied Bias Current Investigation

The applied current that is used for biasing the SOA has also a direct impact on the SOA carrier density and gain. At higher bias current, the larger number of electrons that overcome the energy gap will lead to an increase the carrier density, thus leading to an increased SOA total gain. In Figure 7, the SOA gain reduces with increasing the input signal power and this response appears at all bias current values at 1550 nm wavelength. On the other hand, higher biasing current values result in higher SOA gain achievement. The highest gain achieved is 48 dB with a 40% drop from the steady state value at a bias current of 200 mA and a power of 1 mW. For lower values of bias current, the gain profile is almost flat. For example, injecting the same 1 mW input at 100 mA current, 46.4 dB gain is achieved with just 0.6% drop from steady state. These results correspond to the number of electrons available for amplification in the conduction band.

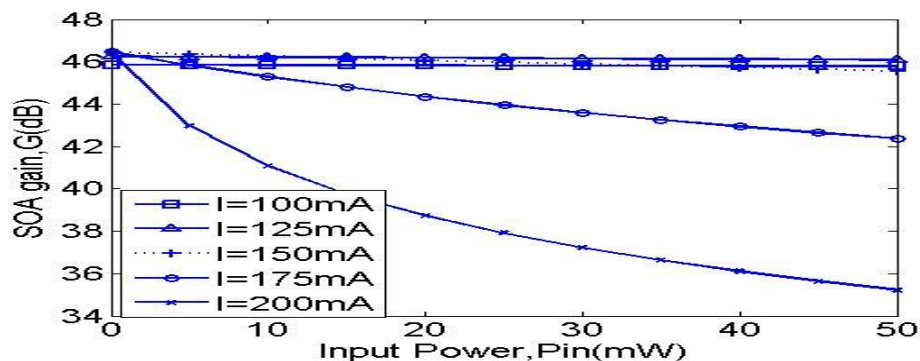


Figure 7. SOA gain *versus* input signal power for a range of bias currents at a wavelength of 1550 nm.

4.4 SOA Length Investigation

The length of the SOA is an important physical parameter that affects the total gain. The dependence of the gain on the SOA length is plotted in Figure 8 for a range of input power values at 150 mA bias current. For short lengths ($< 100 \mu\text{m}$), where the depletion of N is negligible, the gain is the same for all values of P_{in} . On the other hand, for longer lengths ($< 700 \mu\text{m}$), the gain is increasing, peaking at L of $\sim 500 \mu\text{m}$ beyond which the gain drops. The result confirms that the gain is higher for lower values of P_{in} . For longer length ($800 \mu\text{m} - 1.5 \text{ mm}$) SOAs, maintaining a stable applied bias current, the number of electrons per unit length is smaller because of lower current density. Therefore, in order to achieve high gain at longer length SOAs, the applied bias current needs to be increased in order to maintain the number of electrons per unit length.

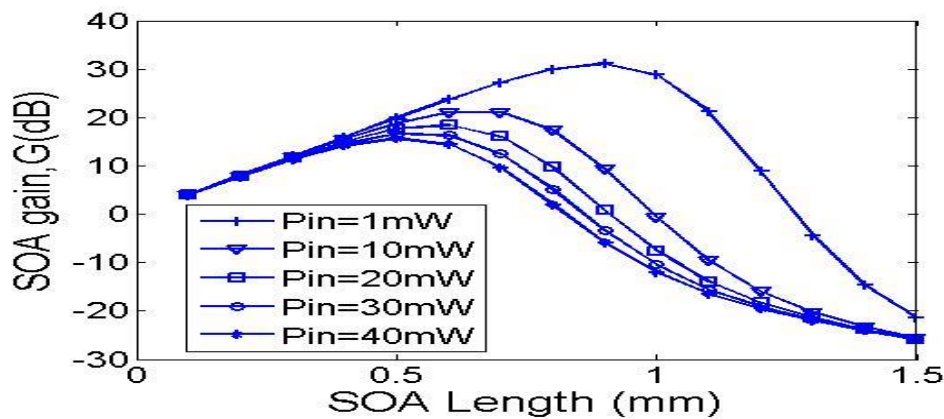


Figure 8. SOA gain responses as a function of SOA length for a range of input power levels with 150 mA bias current.

4.5 Switching

On the contrary to amplification, in order to use cross phase modulation (XPM) and self phase modulation (SPM) characteristics of SOA for the switching function, the signal should experience a phase shift of 180° for the complete deconstructive interference [43]. Therefore, phase shift calculation employing Equations (10), (11), (12) and (13) is crucial for setting the boundaries for the SOA switching function. The phase shift could be induced by the input signal injected to the active region of the SOA.

4.6 Input Signal Wavelength Investigation

The phase shift experienced by the input signal is directly proportional to the depletion of N as defined in (10) and (11). As a result of changes in the refractive index Δn , change is induced in phase shift. Figure 9 shows the phase shift as a function of the input power for a range of wavelengths in the C-band. To achieve an induced phase shift of 180° at 1550 nm wavelength, the input signal power is 60 mW, where the induced phase shift increases with increasing the input power.

4.7 Applied Bias Current Investigation

To explain the effect of bias current on the induced phase shift of the input signal, Figure 10 explains the induced phase shift of the input signal achieved at a range of input power at different biasing current values. From Figure 10, it can be observed that at higher bias current

values, the input signal propagating along the SOA induces more phase shift. Higher biasing results in higher SOA gain. From the third term in (5), which shows the depletion of the carrier density, one can observe that higher gain results in more N depletion. Therefore, the phase shift increases accordingly.

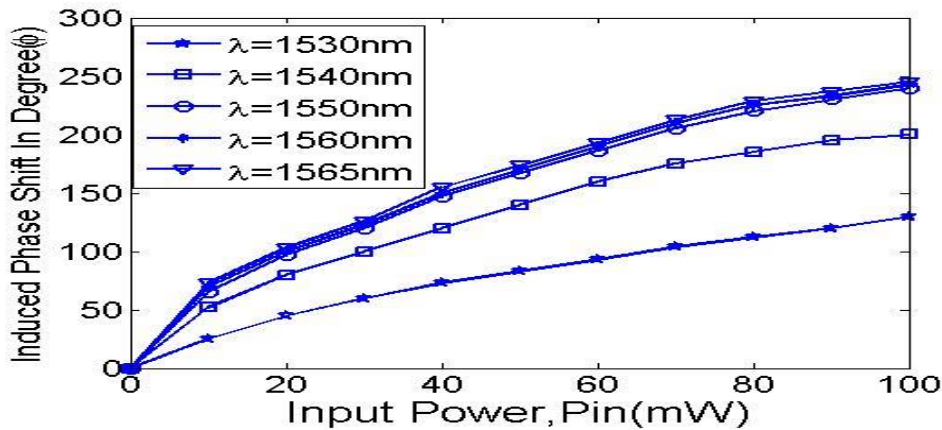


Figure 9. Induced phase shift experienced by the input signal power for a range of wavelengths.

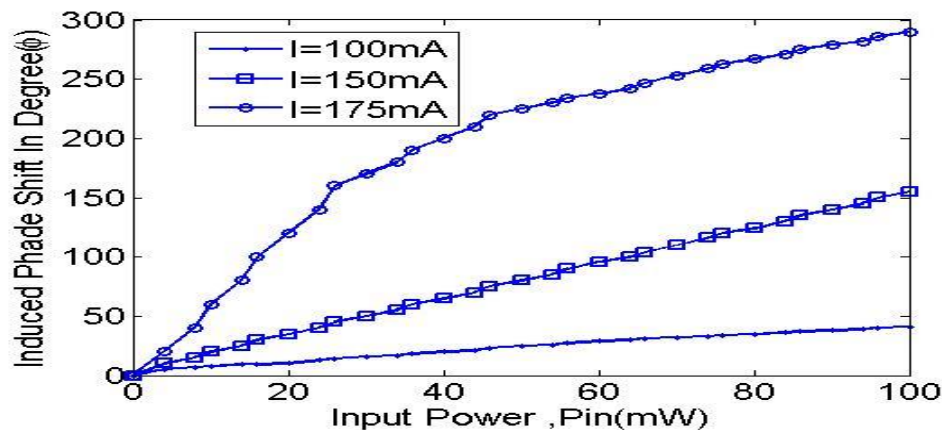


Figure 10. Induced phase shift of the input signal achieved *versus* the input signal power for a range of biasing current values.

4.8 SOA Length Investigation

It is important to explain the dependence of the phase shift of the input signal on the SOA length. It is known that lower gains are achieved at short ($< 100 \mu\text{m}$) and long ($> 700 \mu\text{m}$) SOA lengths. It was shown in Figure 10 that higher input power induces more phase shift, which explains the response in Figure 11. The figure shows the induced phase shift corresponding to the input power at different SOA lengths at 150 mA bias current. It can be concluded that the maximum phase shift is achieved at $500 \mu\text{m}$.

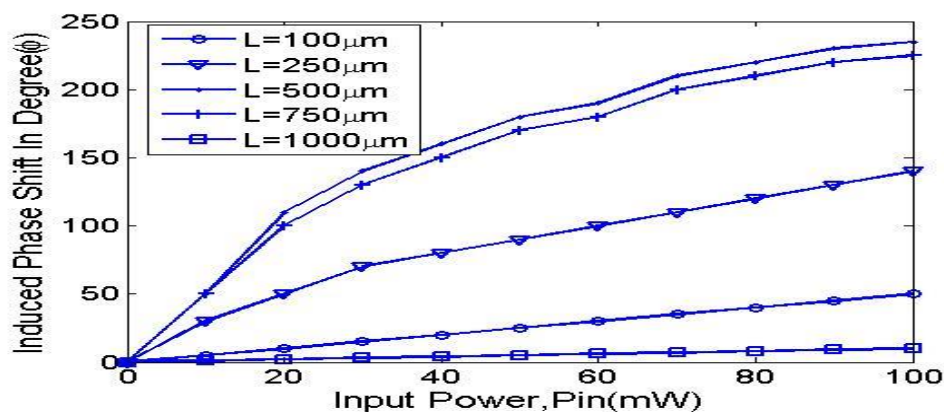


Figure 11. Induced phase shift of the input signal achieved as a function of the input signal power for a range of SOA lengths at 150 mA bias current.

4.9 SOA Temperature Investigation

The temperature of the SOA is an important parameter that affects the total gain and phase shift. The dependence of the gain on the SOA temperature at a wavelength of 1550 nm is shown in Figure 12. It can be noticed that the input signal propagating along the SOA induces the temperature dependence of SOA. The temperature dependence of the peak signal gain is approximately (-0.2) dB/K.

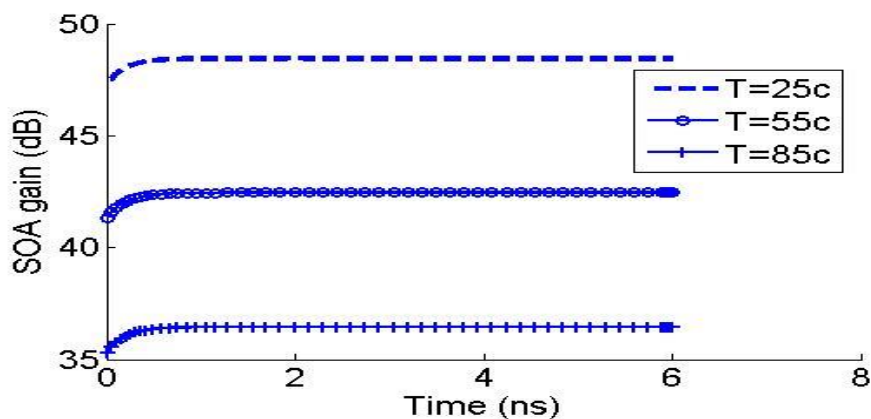


Figure 12. SOA gain corresponding to temperature.

Figure 13 shows that, due to temperature effect on medium gain, the SOA gain decreases with increasing temperature. Such investigation is carried out by using Equations 10, 12 and 13. Temperature can be controlled to obtain a certain phase shift that will become a function of temperature.

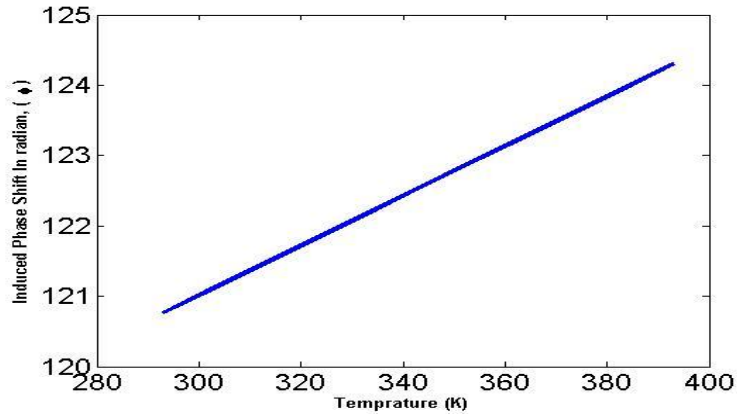


Figure 13. Temperature effect on phase shift.

4.10 Differential Gain Effect

To calculate the saturation power, the following relationship can be used [44]:

$$P_{in(sat)} = \frac{hf}{Go - 2} \frac{2 \ln(2)}{\Gamma} \frac{A}{a_1} \frac{1}{t_c} \quad (14)$$

$$Go = \exp(\Gamma a_1 (N - N_o)) L \quad (15)$$

where Go is the reasonable unsaturated gain, t_c is the effective carrier lifetime.

Figure 14 shows the effect of differential gain on the linearity of the device. Moreover, increasing the differential gain leads to a decrease in the linear region, in terms of 3 dB bandwidth, meaning a decrease in saturation power. On the other hand, decreasing the differential gain leads to an increase in the linear region, meaning an increase in saturation power.

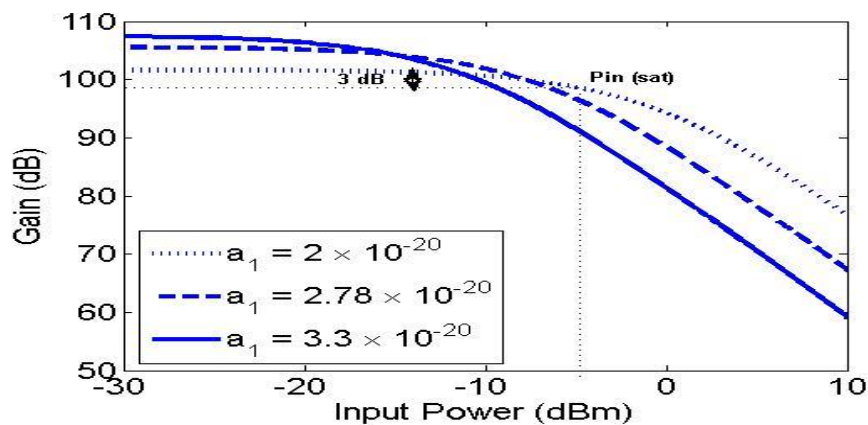


Figure 14. SOA gain as a function of the input power; the 3-dB saturation input power is marked.

5. CONCLUSION

The total gain response of an SOA model using the segmentation method has been simulated. CW probe and pump signals have been applied to the proposed segmentation of SOA model in order to investigate the corresponding gain response. The results have been discussed to achieve amplification and all-optical switching. The optimum performance conditions regarding the input signal power, the bias current and the signal wavelengths have been investigated for the SOA, to function as an amplifier and a switch. Furthermore, thermos-optical effect on total gain and phase shift has been introduced. Moreover, the effect of differential gain on the linear region has been investigated. The model can be extended to investigate vertical cavity SOA.

REFERENCES

- [1] R. Ramaswami and N. Sivarajan, *Optical Network – a Practical Perspective*, 2nd Edition, USA: Morgan Kaufmann, 2002.
- [2] N. S. Bergano, "Wavelength Division Multiplexing in Long-Haul Transoceanic Transmission Systems," *IEEE Journal of Lightwave Technology*, vol. 23, pp. 4125-4139, 2005.
- [3] G. P. Agrawal, *Lightwave Technology - Telecommunication System*, New Jersey, USA: John Wiley and Son, Inc., 2005.
- [4] R. Medina, "Photons vs. Electrons [All-Optical Network]," *Proc. Of the IEEE Potentials*, vol. 21, issue 2, pp. 9-11, May 2002.
- [5] D. Adami, S. Giordano, M. Pagano and L. Gustavo Zuliani, "MCP-RWA: A Novel Algorithm for QOT-Guaranteed Online Provisioning in Photonic Networks," 2010 International Congress on Ultra-Modern Telecommunications and Control Systems and Workshops (ICUMT), pp. 141-147, Moscow, Russia, 18-20 Oct. 2010.
- [6] C. Schubert, J. Berger, S. Diez, H. J. Ehrke, R. Ludwig, U. Feiste, C. Schmidt, H. G. Weber, G. Toptchiyski, S. Randel, Bakopoulos, D. Petrantonakis, G. T. Kanellos, G. Maxwell and H. Avramopoulos, "Optical Signal Processing Using Integrated Multi-Element SOA-MZI Switch Arrays for Packet Switching," *Proc. Of the IET Optoelectronics*, vol. 1, pp. 120-126, 2007.
- [7] E. Kehayas, J. Seoane, Y. Liu, J. M. Martinez, J. Herrera, P. V. Holm Nielsen, S. Zhang, R. McDougall, G. Maxwell, F. Ramos, J. Marti, H. J. S. Dorren, P. Jeppesen and H. Avramopoulos, "All-Optical Network Subsystems Using Integrated SOA-Based Optical Gates and Flip-Flops for Label-Swapped Networks," *Proc. of the IEEE Photonics Technology Letters*, vol. 18, pp. 1750-1752, 2006.
- [8] S. L. Jansen, S. Spalter, G. D. Khoe, W. Huug de, H. E. Escobar, L. Marshall and M. Sher, "16x40 gb/s over 800 km of SSMF Using Midlink Spectral Inversion," *Proc. of the IEEE Photonics Technology Letters*, vol. 16, pp. 1763-1765, 2004.
- [9] A. Barbieri, G. Colavolpe, T. Foggi, E. Forestieri and G. Prati, "OFDM *versus* Single-Carrier Transmission for 100 Gbps Optical Communication," *Proc. of the IEEE, Journal of Lightwave Technology*, vol. 28, pp. 2537-2551, 2010.
- [10] A. Paraskevopoulos, S. H. Voss, M. Talmi and G. Walf, "High Speed (>100 Gbps) Key Components for a Scalable Optical Data Link, to be Implemented in Future Maskless Lithography Applications," *Proc. of the 25th European Mask and Lithography Conference (EMLC)*, pp. 1-8, 2009.
- [11] H. Uemura, H. Hamasaki, H. Furuyama, H. Numata, C. Takubo and H. Shibata, "Extremely-Compact and High-Performance (160Gbps = 20GB/s) Optical Semiconductor Module Using Lead Frame Embedded Optoelectronic Ferrule", *Proc. of the 58th Conference on Electronic Components and Technology (ECTC 2008)*, pp. 1936-1940, 2008.
- [12] A. V. Nguyen, H. P. Nguyen, N. B. Le and V. L. Dang, "Digital Lightwave Receiver Employing Parallel-DSP-Based Equalization Technique for 100 Gbps 1000-km RZ-DQPSK Optical

- Communication System," Proc. of International Conference on Advanced Technologies for Communications (ATC), pp. 152-155, 2011.
- [13] J. M. Martinez, J. Herrera, F. Ramos and J. Marti, "All-Optical Correlation Using Cascaded Logic XOR Gates Based on Active Mach-Zehnder Interferometers," Proc. of the 31st European Conference on Optical Communication (ECOC 2005), vol. 1, pp. 103-104, 2005.
- [14] J. Leuthold, P. A. Besse, J. Eckner, E. Gamper, M. Dulk and H. Melchior, "All-Optical Space Switches with Gain and Principally Ideal Extinction Ratios," Proc. of the IEEE, Journal of Quantum Electronics, vol. 34, pp. 622-633, 1998.
- [15] K. Morito, J. Leuthold and H. Melchior, "Dynamic Analysis of MZI-SOA All-Optical Switches for Balanced Switching," Proc. of the 11th International Conference on Integrated Optics and Optical Fiber Communications, and 23rd European Conference on Optical Communications (Conf. Publ. No.: 448), vol. 2, pp. 81-84, 1997.
- [16] N. Pleros, P. Zakynthinos, A. Poustie, D. Tsiokos, P. Bakopoulos, D. Petrantonakis, G. T. Kanellos, G. Maxwell and H. Avramopoulos, "Optical Signal Processing Using Integrated Multi-Element SOA-MZI Switch Arrays for Packet Switching," Proc. of the IET Optoelectronics, vol. 1, pp. 120-126, 2007.
- [17] A. Maziotis, B. Schrenk, M. Bougioukos and H. Avramopoulos, "Cognitive Routing in Converged Access-Metro Environment via Selective SOA-MZI Switch," Proc. of the IEEE Photonics Technology Letters, pp. 1-1, 2011.
- [18] D. Petrantonakis, D. Apostolopoulos, M. Spyropoulou, N. Pleros, K. Vysokinos and H. Avramopoulos, "40 Gb/s NRZ Wavelength Conversion with Enhanced 2R Regeneration Characteristics Using a Differentially-Biased SOA-MZI Switch," LEOS Annual Meeting Conference Proceedings of IEEE (LEOS '09), pp. 781-782, 2009.
- [19] J. Kurumida, Y. Tatara, H. Uenohara and K. Kobayashi, "All-Optical Header Recognition Sub-System Based on SOA-MZI Switches," Proc. of Conference on Lasers and Electro-Optics Pacific Rim (CLEO/Pacific Rim), pp. 1790- 1791, 2005.
- [20] S. Gupta, M. Presi, N. Calabretta, G. Contestabile and E. Ciaramella, "Operational Equivalence of Self-Switching Effect in SOA-Based Nonlinear Polarization and MZI Switches," Proc. in: Lasers and Electro-Optics Society, LEOS, 20th Annual Meeting of IEEE, pp. 810-811, 2007.
- [21] S. Nakamura, K. Tajima and Y. Sugimoto, "Experimental Investigation on High-speed Switching Characteristics of A Novel Symmetric Mach-Zehnder All-Optical Switch," Applied Physics Letter, vol. 65, pp. 283-385.
- [22] G. P. Agrawal, "Population Pulsations and Non-degenerate Four-Wave Mixing in Semiconductor Lasers and Amplifiers," J. Opt. Soc. Am. B, vol. 5, no. 1, pp. 147– 159, 1988.
- [23] C. Cheng, X. Zhang, Y. Zhang, L. Liu and D. Huang, "Measurement of the Carrier Recovery Time in SOA Based on Dual Pump FWM," Proc. in: Communications and Photonics Conference and Exhibition (ACP), Asia, pp. 1-2, 2009.
- [24] H. Le Minh, Z. Ghassemlooy and N. Wai Pang, "Characterization and Performance Analysis of a TOAD Switch Employing a Dual Control Pulse Scheme in High-speed OTDM Demultiplexer," Proc. of the IEEE Communications Letters, vol. 12, pp. 316-318, 2008.
- [25] J. M. Tang, P. S. Spencer, P. Rees and K. A. Shore, "Enhanced TOAD Performance by Negative Frequency-Detuned Signal and Control Picoseconds Optical Pulses," Proc. of the IEEE Journal of Quantum Electronics, vol. 36, pp. 574-582, 2000.
- [26] J. Wei, Z. Min and P. Ye, "All-Optical-Packet Header and Payload Separation for Unslotted Optical-Packet-Switched Networks," Proc of the IEEE Journal of Lightwave Technology, vol. 25, pp. 703-709, 2007.
- [27] E. S. Awad, C. J. K. Richardson, P. S. Cho, N. Moulton and J. Goldhar, "Optical Clock Recovery Using SOA for Relative Timing Extraction between Counterpropagating Short Picosecond Pulses," Proc. of the IEEE Photonics Technology Letters, vol. 14, pp. 396-398, 2002.

- [28] R. Giller, R. J. Manning and D. Cotter, "Gain and Phase Recovery of Optically Excited Semiconductor Optical Amplifiers," *Proc. of the IEEE Photonics Technology Letters*, vol. 18, pp. 1061-1063, 2006.
- [29] J. Moerk, M. Nielsen and T. Berg, "The Dynamics of Semiconductor Optical Amplifiers-Modeling and Applications," *Proc. in: Optics and Photonics News*, vol. 14, pp. 42-48, 2003.
- [30] E. Tangdionga, Y. Liu, H. Waardt, G. Khoe, A. Koonen and H. Dorren, "All-Optical Demultiplexing of 640 to 40 Gbits/s Using Filtered Chirp of a Semiconductor Optical Amplifier," *Proc. of the Optics Letters*, vol. 32, pp. 835-837, 2007.
- [31] A. Perez-Pardo, T. T. Ng, P. Petropoulos, S. Sales and D. J. Richardson, "Analysis of the Dynamic Responses of SOA Wavelength Converters Using Linear Frequency Resolved Gating Technique," *Proc. of the IEEE Photonics Technology Letters*, vol. 20, pp. 1079-1081, 2008.
- [32] M. Matsuura, N. Kishi and T. Miki, "All-Optical Wavelength Conversion with Large Wavelength Hopping by Utilizing Multistage Cascaded SOA-Based Wavelength Converters," *Proc. of the IEEE Photonics Technology Letters*, vol. 18, pp. 926-928, 2006.
- [33] T. Kise, K. N. Nguyen, J. M. Garcia, H. N. Poulsen and D. J. Blumenthal, "Demonstration of Cascadability and Phase Regeneration of SOA-Based All-Optical DPSK Wavelength Converters," *Proc. of the Optical Fiber Communication Conference and Exposition (OFC/NFOEC) and the National Fiber Optic Engineers Conference*, pp. 1-3, 2011.
- [34] L. Pei-Li, H. De-Xiu and Z. Xin-Liang, "SOA-Based Ultra-fast Multifunctional All-Optical Logic Gates with PolSK Modulated Signals," *Proc. of the IEEE Journal of Quantum Electronics*, vol. 45, pp. 1542-1550, 2009.
- [35] J. Moerk, M. Nielsen and T. Berg, "The Dynamics of Semiconductor Optical Amplifiers-Modeling and Applications," *Proc. of the Optics and Photonics News*, vol. 14, pp. 42-48, 2003.
- [36] E. S. Awad, C. J. K. Richardson, P. S. Cho, N. Moulton and J. Goldhar, "Optical Clock Recovery Using SOA for Relative Timing Extraction between Counterpropagating Short Picosecond Pulses," *Proc. of the IEEE Photonics Technology Letters*, vol. 14, pp. 396-398, 2002.
- [37] H. Le Minh, "All-Optical Router with PPM Header Processing High-Speed Photonic Packet Switching Networks," North Umbria University, 2007.
- [38] M. Y. Jeon, Y. A. Leem, D. C. Kim, E. Sin, S. B. Kim, H. Ko, D. S. Yee and K. H. Park, "40 Gbps All-Optical 3R Regeneration and Format Conversion with Related InP-Based Semiconductor Devices," *Proc. of the ETRI Journal*, vol. 29, no. 5, pp. 633-640, Oct. 2007.
- [39] H. Wang, J. Wu and J. Lin, "Studies on the Material Transparent Light in Semiconductor Optical Amplifiers," *Proc. of the Journal of Optics A: Pure and Applied Optics*, vol. 7, pp. 479-492, 2005.
- [40] F. Marino, G. Catalan, P. Sánchez, O. Piro and S. Balle, "Thermo-optical Canards and Excitable Limit Cycles," *Physical Review Letter*, vol. 92, 073901, Feb. 2004.
- [41] Bradley J. Frey, Douglas B. Leviton and Timothy J. Madison, "Temperature-Dependent Refractive Index of Silicon and Germanium," NASA Goddard Space Flight Center, Greenbelt, MD 20771.
- [42] A. Abd El Aziz, W. P. Ng, Z. Ghassemlooy, M. H. Aly, R. Ngah and M. F. Chaing, "Characterization of the Semiconductor Optical Amplifier for Amplification and Photonic Switching Employing the Segmentation Model," *International Conference on Transparent Optical Networks "Mediterranean Winter" 2008 (ICTON-MW'08)*, ISBN 978-1-4244-3485-5, Marrakech, Morocco, pp. Fr1A.1 (1-6), 11-13 Dec. 2008.
- [43] G. P. Agrawal and N. A. Olsson, "Self-Phase Modulation and Spectral Broadening of Optical Pulses in Semiconductor Laser Amplifiers," *Proc. of the IEEE Journal of Quantum Electronics*, vol. 25, pp. 2297-2306, 1989.

- [44] R. Bonk, T. Vallaitis, J. Guetlein, C. Meuer, H. Schmeckeber, D. Bimberg, C. Koos, W. Freude and J. Leuthold, "The Input Power Dynamic Range of a Semiconductor Optical Amplifier and Its Relevance for Access Network Applications," Proc. of the IEEE Photonics Journal, vol. 3, no. 6, December 2011.

ملخص البحث:

يعالج هذا البحث تأثيرات إشارة الدخل في مقدار الكسب و كثافة الناقل في المكبر الضوئي شبه الموصل. تمت نمذجة المكبر الضوئي شبه الموصل باستخدام طريقة التجزئة؛ وأخذ بعين الاعتبار كل من تيار انحياز الدخل، و قدرة الدخل، و الطول الموجي، و طول المكبر اللازمة لعمل المكبر الضوئي شبه الموصل في حالتها التكبير و التبديل. علاوة على ذلك، جرى استقصاء تأثير درجة الحرارة على عمل المكبر الضوئي شبه الموصل، كما تمت دراسة الأثر الحراري الضوئي.

و قد أظهرت محاكاة مبدأ التشغيل الشروط و المتطلبات الحديثة للدخل التي يمكن عندها استخدام المكبر الضوئي شبه الموصل كمكبر و مبدل.



This article is an open access article distributed under the terms and conditions of the Creative Commons Attribution (CC BY) license (<http://creativecommons.org/licenses/by/4.0/>).